

Frictional drag between superconducting $\text{LaAlO}_3/\text{SrTiO}_3$ nanowires

Yuhe Tang,^{1,2} Jung-Woo Lee,³ Anthony Tylan-Tyler,^{1,2} Hyungwoo Lee,³ Michelle Tomczyk,^{1,2} Mengchen Huang,^{1,2} Chang-Beom Eom,³ Patrick Irvin,^{1,2} and Jeremy Levy^{1,2}

¹*Department of Physics and Astronomy,*

University of Pittsburgh, Pittsburgh, Pennsylvania 15260, USA

²*Pittsburgh Quantum Institute, Pittsburgh, Pennsylvania 15260, USA*

³*Department of Materials Science and Engineering,*

University of Wisconsin-Madison, Madison, Wisconsin 53706, USA

Abstract

We report frictional drag measurements between two superconducting $\text{LaAlO}_3/\text{SrTiO}_3$ nanowires. In these experiments, current passing through one nanowire induces a voltage across a nearby electrically isolated nanowire. The frictional drag signal contains both symmetric and antisymmetric components. The antisymmetric component arises from the rectification of quantum shot noise in the drive nanowire by the broken symmetry in the drag nanowire. The symmetric component in the drag resistance is ascribed to rectification of thermal noise in the drive nanowire during superconducting-normal transition. The suppression of the symmetric component is observed when a normal nanowire is used as either a drag or drive nanowire with the other nanowire superconducting. The absence of symmetric drag resistance between a normal drag nanowire and a superconducting drive nanowire suggests a higher electron-hole asymmetry in the superconducting $\text{LaAlO}_3/\text{SrTiO}_3$ nanowire arising from the 1D nature of superconductivity at $\text{LaAlO}_3/\text{SrTiO}_3$ interface.

SrTiO₃ (STO) has long attracted interest as a superconducting semiconductor [1–3]. Recently, interest in the superconducting properties of STO was revived by the development of STO-based heterostructures and nanostructures and with the LaAlO₃/SrTiO₃ (LAO/STO) system [4] in particular. The LAO/STO two-dimensional interface supports superconductivity, which is electrostatically gateable, and various transport techniques have been used to study the superconductivity at the interface [5]. The superconducting transition temperature (T_C) has a dome shape as a function of carrier density, which is controllable via a backgate [6]. With the use of conductive-atomic force microscope (c-AFM) lithography, nanoscale control over the conductance of the LAO/STO interface is possible. This technique relies on AFM tip-controlled protonation or deprotonation of the LAO surface, which enables the creation of a wide variety of quantum-confined structures, including superconducting nanowires [7], ballistic 1D electron waveguides [8], and single-electron transistors [9, 10]. These mesoscopic devices, drawn from a well-established toolset of quantum transport, often exhibit surprising new properties due to the unique physics of the STO interface such as electron pairing without forming superconductivity [10]. Recently by studying the superconductivity in LAO/STO nanowires of different widths and numbers, it is discovered that superconductivity exists at the boundary of nanowires and is absent within the interior region of nanowires, which indicates the 1D nature of superconductivity at LAO/STO interface [3].

Coulomb drag [11], or more generally frictional drag, first proposed by Pogrebinskii [12], has proven to be a powerful technique to study electron transport and electron correlations. When two electrical conductors are placed in close proximity, current driven through one (“drive”) conductor may induce a voltage (or current) in the second (“drag”) conductor. Frictional drag measurements have mostly been carried out between normal state conductors in coupled 2D semiconductor systems [13–17], graphene systems [18, 19], 1D semiconductor systems [20–22], 1D complex oxide systems [23], and quantum dot systems [24]. Frictional drag in the superconducting regime has been carried out in normal metal-superconductor systems [25, 26] and the phenomenon is explained by the local fluctuating electric field induced by mobile vortices in the superconducting layer [27] or Coulomb coupling between two conductors. [28, 29]. There are, to our knowledge, no prior reports of frictional drag between two quasi-1D superconductors.

Previously-reported frictional drag experiments at the LAO/STO-based nanowires have

shown surprising results, particularly in the high magnetic field regime [23]. The drag resistance is anti-symmetric, indicating that the drag resistance arises via rectification of quantum shot noise in the drive nanowire due to the broken inversion symmetry of the drag nanowire [30]. Remarkably, the drag resistance shows little to no dependence on the separation between nanowires (up to $\sim \mu\text{m}$ scales). This unusual scaling strongly indicates that non-Coulombic interactions dominate the coupling between these nanowires.

Here we report frictional drag experiments between two LAO/STO superconducting nanowires. The drag resistance contains a mixture of symmetric and anti-symmetric components and the symmetric component disappears whenever one nanowire is normal and the other is superconducting. The antisymmetric component arises for the same reasons as in the high B regime. The symmetric component is ascribed to the rectification of thermal noise in the drive nanowire during the superconducting-normal transition. Suppression of the symmetric drag component, when a normal nanowire is used as the drag nanowire, suggests the existence of a higher electron-hole asymmetry [31] in the superconducting LAO/STO nanowires arises from the 1D nature of superconductivity at LAO/STO interface.

Nanowire devices are “sketched” on LAO/STO heterostructures using c-AFM lithography [32] (Fig. 1(a)). LAO/STO heterostructures with an LAO thickness of 3.4 unit cells are grown by pulsed laser deposition (PLD). Further details of the sample growth and the device fabrication process are described elsewhere [33]. The width of the nanowires used for these experiments is approximately $w = 10$ nm, as quantified by erasure experiments [32]. Other device parameters include the separation between nanowires d and the nanowire length L . Here we focus on two sets of parameters: $d = 40$ nm and $L = 400$ nm (device 2B, Fig. 2) and $d = 40$ nm and $L = 300$ nm (device 2J, Fig. 4). To investigate frictional drag at the LAO/STO interface in the superconducting regime, the magnitude of B is kept below 0.3 T and the temperature less than 100 mK (except for temperature-dependent measurements that explicitly go above $T = 100$ mK). In a frictional drag experiment, a voltage V_i in nanowire i is induced by a current I_j in nanowire j (Fig. 1(b)). All nanowires are connected to the same ground during the measurement. The current I_j is produced by applying a voltage $V_{Sj} = V_{\text{DC}} + V_{\text{AC}} \cos \omega t$ to one end of nanowire j ; the resulting current $I_j(\omega)$ and induced voltage $V_j(\omega)$ at frequency ω are measured using a lock-in amplifier. The resistance may then be expressed as a matrix $R_{ij} = dV_i/dI_j = V_i(\omega)/I_j(\omega)$, which is generally a function of the DC drive current I_j (as well as other parameters such as temperature T

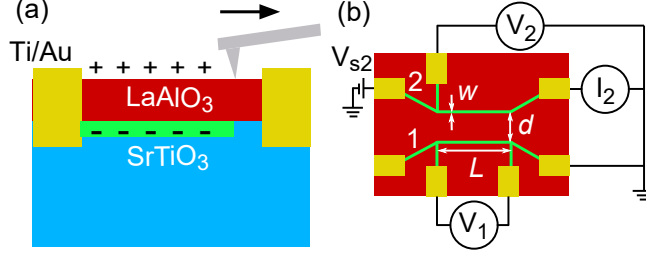


FIG. 1. Experimental setup. (a) Side-view of the nanowire fabrication process. A nanowire is created at the LAO/STO interface between two Ti/Au electrical contacts with c-AFM lithography. Protons (+) patterned on the surface by the AFM tip attract electrons (-) to the interface forming a nanowire (green area). (b) Top-view schematic of the double nanowire device with length L , width w , and nanowire separation d . The setup measures the induced drag voltage V_1 across nanowire 1 created by current I_2 , which is induced by application of a voltage V_{S2} across nanowire 2.

and applied magnetic field \vec{B}). The off-diagonal terms then define the drag resistance R_{ij} characterize the mutual friction between electrons in the drive and drag nanowires. In order to ensure that the drag resistances R_{ij} are not influenced by current leakage between the two nanowires, all measurements are performed well below the inter-wire breakdown voltage (~ 10 V) measured for each device.

Typical frictional drag resistance measurements in the superconducting regime are shown in Fig. 2. Both nanowires in device 2B show signatures of superconductivity [7]. As shown in the bottom panels of Fig. 2(a) and (b), nanowire 2 displays three superconducting-normal transitions with critical current I_c defined as the location of the peaks in $R_{2T,2}$ [7]. The first is at ± 20 nA, the second at ± 110 nA, and the third at ± 140 nA. Non-vanishing resistances in superconducting nanowires are common and are attributed to normal hotspots below I_c [34] or quantum phase slips [25]. The superconducting-normal transition at ± 20 nA arises from the nanowire since it shows up both in $R_{2T,2}$ and four-terminal resistance R_{22} and the transition at ± 110 nA and ± 140 nA arises from wires connecting the nanowire and electrodes since it only shows up in $R_{2T,2}$ (Fig. S1). The drag resistance R_{12} is greatly enhanced in the superconducting regime, as can be seen by examining both the temperature-dependence (Fig. 2(c)) and the magnetic-field dependence (Fig. 2(d)). The nature of R_{12} in the superconducting regime is qualitatively different from the high magnetic field regime (where the nanowires are not superconducting). In the high magnetic field regime, the

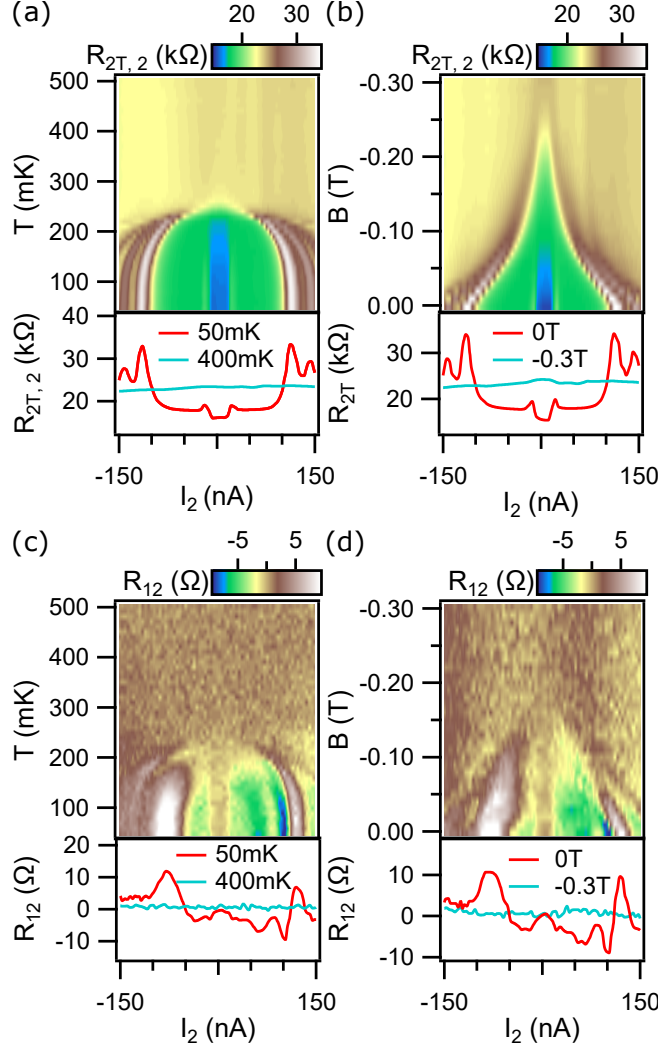


FIG. 2. Temperature and magnetic-field dependence of the drag resistance and two-terminal resistance of the drive nanowire. (a) Temperature dependence and line profiles of the drive nanowire's two-terminal resistance $R_{2T,2}$ from nanowire 2. Top panel, temperature dependence of drag resistance R_{12} from nanowire 1. Bottom panel, line profiles of R_{12} at 50 mK and 400 mK. (b) Magnetic field dependence and line profiles of the drive nanowire's two-terminal resistance $R_{2T,2}$. (c) Temperature dependence and line profiles of drag resistance R_{12} from nanowire 1. (d) Magnetic field dependence and line profiles of drag resistance R_{12} .

drag resistance R_{ij} is antisymmetric [23] with respect to the sourcing current, while the superconducting response is asymmetric with drive current. The superconducting R_{ij} is mostly symmetric between $I_2 = \pm 40$ nA with two tiny dips at ± 10 nA. As the magnitude of I_2 increases, an anti-symmetric component starts showing up in R_{ij} and R_{ij} becomes

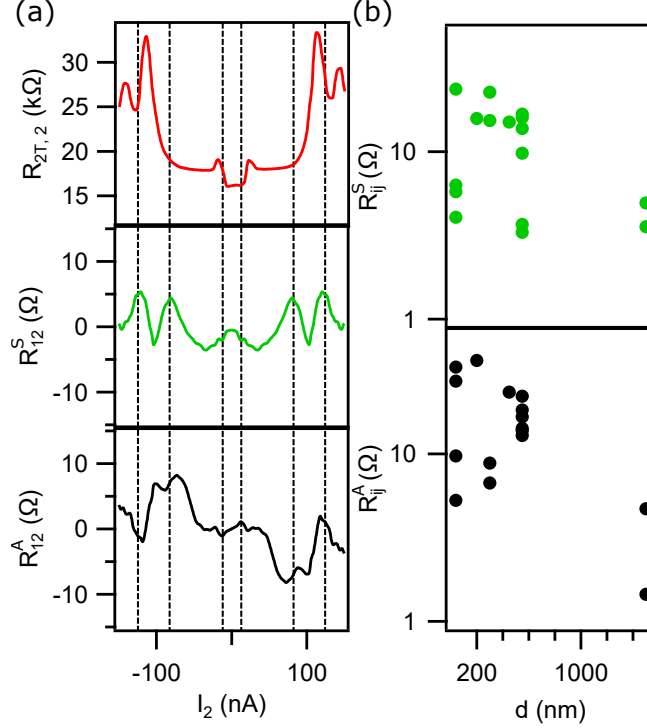


FIG. 3. Symmetric and anti-symmetric components of drag resistance. (a) Typical symmetric and anti-symmetric components of drag resistance from device 2B. Top panel: Two-terminal resistance $R_{2T,2}$ of drive nanowire. Middle panel: Symmetric component of drag resistance R_{12} . Bottom panel: Anti-symmetric component of drag resistance R_{12} . (b) d dependence of symmetric and anti-symmetric components. d ranges from 40nm to 1.5 μ m. Top panel: Symmetric component R_{ij}^S as a function of d . Bottom panel: Anti-symmetric component R_{ij}^A as a function of d .

asymmetric.

The appearance of asymmetric R_{12} (Fig. 2(c) and (d)) in the superconducting regime is correlated with the superconductivity in the drive nanowire 2 (Fig. 2(a) and (b)). To further understand the frictional drag in the superconducting regime, we extract symmetric and anti-symmetric components by $R_{ij}^S(I) = (R_{ij}(I) + R_{ij}(-I))/2$ and $R_{ij}^A(I) = (R_{ij}(I) - R_{ij}(-I))/2$. $R_{2T,2}$, R_{ij}^S and R_{ij}^A are shown in top, middle and bottom panels of Fig. 3(a). Dashed lines pinpoint locally strongest drag resistance in R_{12}^S . As shown in Fig. 3(a), locally strongest R_{12}^S show up around the superconducting-normal transition represented by peaks in $R_{2T,2}$ in the drive nanowire 2 accompanied by locally strongest R_{12}^A . The nature of coupling between nanowires for R_{ij}^S and R_{ij}^A is still unknown. But according to devices with d ranging from 40nm to 1.5 μ m, both R_{ij}^S and R_{ij}^A persist over large separations and are nearly independent

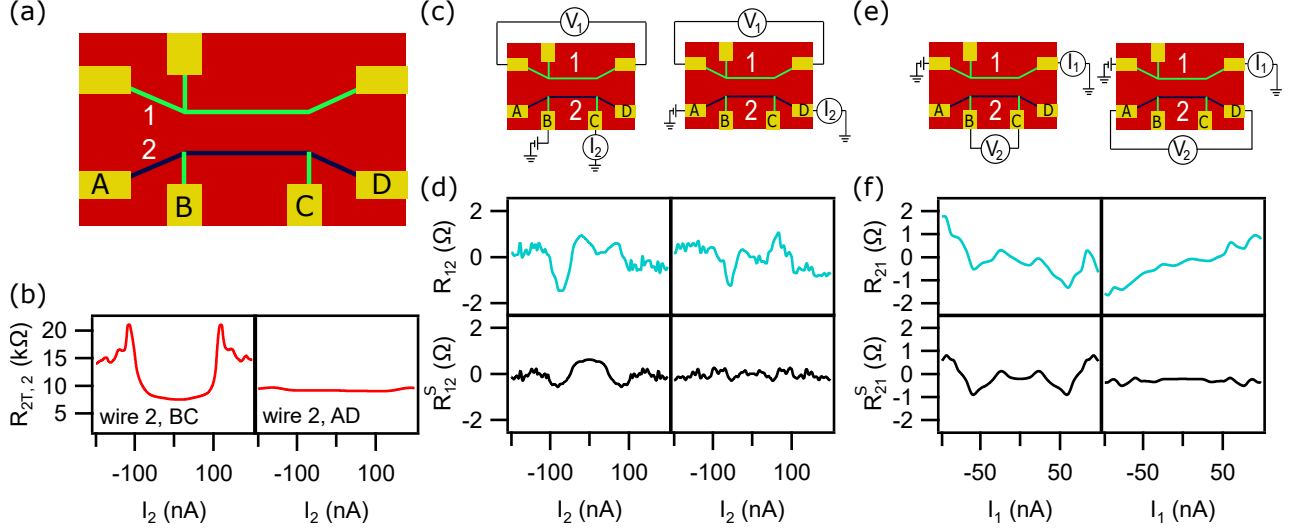


FIG. 4. Frictional drag in the superconducting regime with one normal-state nanowire. (a) Schematic of the device with normal-state nanowire. Black sections in nanowire 2 are normal; green sections in nanowire 2 and 1 are superconducting. (b) Left: Two terminal resistance of nanowire 2 measured between B and C. Superconductivity arises from the green portions as shown in panel (a). Right: Two terminal resistance of nanowire 2 between A and D when the whole nanowire is in normal state. (c) Measurement configurations when nanowire 2 is used as the drive nanowire. (d) Drag resistance R_{12} and its symmetric component R_{12}^S . Left and right panels correspond to the measurement configuration in (c). (e) Measurement configurations when nanowire 2 is used as the drag nanowire. (f) Drag resistance R_{21} and its symmetric component R_{21}^S . Left and right panels correspond to the measurement configurations in (e).

of d (Fig. 3(b)). Since the $e^{-4k_F d}$ behavior is not observed in both R_{ij}^S and R_{ij}^A , where $k_F \sim (10\text{nm})^{-1}$ is the Fermi wave vector, the Coulomb coupling can be ruled out as the dominating effect [35].

To corroborate that the symmetric component of drag resistance is related to the superconducting-normal transition in the drive nanowire, we examine the drag resistance from devices with one superconducting nanowire and one normal nanowire. The superconducting properties of LAO/STO is known to be gate-tunable both in 2D geometries [36] and in 1D [3, 7]. There are known inhomogeneities in electron density which most likely arise from the underlying ferroelastic domain structure[37]. While we cannot independently control the carrier density of one nanowire while keeping the second fixed, we can select

devices in which one nanowire shows superconducting behavior and the other does not. Fig. 4 shows the typical data from Device 2J. As illustrated in Fig. 4(a), green-colored nanowires are superconducting, while black nanowires are in the normal-state. The information about the state of the nanowires is inferred from two-terminal resistance measurements (Fig. 4(b)). We then can compare the frictional drag as sensed by nanowire 1 due to two configurations—one in which one device contains a superconducting section and one in which the other does not.

First we consider the configuration where superconducting nanowire 1 is the drag nanowire and examine the influence of drive nanowire's state on drag resistance, as shown in Fig. 4(c). When both the drive and drag nanowires are superconducting, the drag resistance R_{12} is asymmetric (Fig. 4(d) left top panel) with a large symmetric component (Fig. 4(d) left bottom panel). However, when the drive nanowire is normal, the drag resistance is mostly anti-symmetric (Fig. 4(d) right top panel) with a negligible symmetric component (Fig. 4(d) right bottom panel).

The symmetric component of drag resistance showing up around the superconducting-normal transition in the drive nanowire can be explained by the rectification of the thermal noise in the drive nanowire [30] which requires electron-hole asymmetry in both drive and drag nanowires. When a superconducting nanowire undergoes superconducting-normal transition, the nanowire's resistance increases. This process generates thermal energy, which in turn gives rise to a large thermal noise and a greatly enhanced symmetric component of drag resistance. For the normal nanowire, therefore there is no significant enhancement of the thermal noise, and the symmetric component of drag resistance remains small at all biases across the drive nanowire.

The rectification of thermal noise in the drive also explains the strong correlation between R_{12}^A and R_{12}^S . R_{12}^A comes from the rectification of the shot noise in the drive nanowire [23]. Shot noise is a non-equilibrium phenomenon depending on the voltage bias across the drive nanowire [30]. During the superconducting-normal transition in the drive nanowire, the change of drive nanowire's resistance changes the bias across different portions of the nanowire, thus inducing quantum shot noise and anti-symmetric R_{ij} is observed simultaneously with symmetric drag resistance.

The symmetric component in drag resistance is also strongly suppressed when the drag nanowire is in the normal state. As shown in the left panel of Fig. 4(e), when the drag

resistance is measured between B and C of nanowire 2, the drag resistance R_{21} is asymmetric with a large symmetric component (Fig. 4(f) left). However when the drag resistance is measured between A and D, the drag resistance is anti-symmetric with a negligible symmetric component. Since the drive nanowire 1 is superconducting in both configurations, the absence of symmetric drag resistance component with a normal drag nanowire cannot be ascribed to the absence of thermal noise in the drive nanowire. The magnitude of symmetric drag resistance depends on the electron-hole asymmetry in the drag nanowire [11]. The fact that the symmetric drag resistance measured from a superconducting drag nanowire is larger may be explained by the electron-hole asymmetry is stronger in superconducting nanowire than normal nanowire. Electron-hole symmetry is more easily broken in low dimensional devices [30, 31]. It is reported that the superconductivity at LAO/STO interface is 1D in nature situated at the boundary of the nanowire and is absent within the interior region of the nanowire [3]. Thus the overall dimension of the nanowire is reduced as it becomes superconducting compared to a normal nanowire due to the formation of 1D superconducting boundary. This reduced dimension of the nanowire gives rise to a stronger electron-hole asymmetry. Therefore the symmetric component of drag resistance is stronger measured from a superconducting drag nanowire.

In summary, frictional drag between superconducting LAO/STO nanowires exhibits a strong and highly symmetric component in drag resistance, which is distinct from the anti-symmetric drag resistance between LAO/STO nanowires in the normal state. The symmetric component arises from rectification of thermal noise in the drive superconducting nanowire based on the fact that it shows up at the vicinity of superconducting-normal transition in the drive nanowire and disappears when the drive nanowire is normal. The symmetric component in drag resistance also disappears when the drag nanowire is normal, which can be attributed to the 1D nature of superconductivity in LAO/STO systems.

Work at the University of Pittsburgh was supported by funding from the DOE Office of Basic Energy Sciences under award number DOE de-sc0014417. The work at the UW-Madison (synthesis and characterizations of thin films heterostructures) was supported by the US Department of Energy (DOE), Office of Science, Office of Basic Energy Sciences (BES), under award number DE-FG02-06ER46327.

-
- [1] J. Schooley, W. Hosler, and M. L. Cohen, Physical Review Letters **12**, 474 (1964).
 - [2] X. Lin, Z. Zhu, B. Fauqué, and K. Behnia, Physical Review X **3**, 021002 (2013).
 - [3] Y.-Y. Pai, H. Lee, J.-W. Lee, A. Annadi, G. Cheng, S. Lu, M. Tomczyk, M. Huang, C.-B. Eom, P. Irvin, *et al.*, Physical review letters **120**, 147001 (2018).
 - [4] A. Ohtomo and H. Hwang, Nature **427**, 423 (2004).
 - [5] C. Richter, H. Boschker, W. Dietsche, E. Fillis-Tsirakis, R. Jany, F. Loder, L. Kourkoutis, D. Muller, J. Kirtley, C. Schneider, *et al.*, Nature **502**, 528 (2013).
 - [6] A. Caviglia, S. Gariglio, N. Reyren, D. Jaccard, T. Schneider, M. Gabay, S. Thiel, G. Hammerl, J. Mannhart, and J.-M. Triscone, Nature **456**, 624 (2008).
 - [7] J. P. Veazey, G. Cheng, P. Irvin, C. Cen, D. F. Bogorin, F. Bi, M. Huang, C.-W. Bark, S. Ryu, K.-H. Cho, *et al.*, Nanotechnology **24**, 375201 (2013).
 - [8] A. Annadi, G. Cheng, H. Lee, J.-W. Lee, S. Lu, A. Tylan-Tyler, M. Briggeman, M. Tomczyk, M. Huang, D. Pekker, *et al.*, Nano letters **18**, 4473 (2018).
 - [9] G. Cheng, P. F. Siles, F. Bi, C. Cen, D. F. Bogorin, C. W. Bark, C. M. Folkman, J.-W. Park, C.-B. Eom, G. Medeiros-Ribeiro, *et al.*, Nature Nanotechnology **6**, 343 (2011).
 - [10] G. Cheng, M. Tomczyk, S. Lu, J. P. Veazey, M. Huang, P. Irvin, S. Ryu, H. Lee, C.-B. Eom, C. S. Hellberg, and J. Levy, Nature **521**, 196 (2015).
 - [11] B. Narozhny and A. Levchenko, Reviews of Modern Physics **88**, 025003 (2016).
 - [12] M. Pogrebinskii, Soviet Physics-Semiconductors **11**, 372 (1977).
 - [13] T. Gramila, J. Eisenstein, A. MacDonald, L. Pfeiffer, and K. West, Physical review letters **66**, 1216 (1991).
 - [14] T. Gramila, J. Eisenstein, A. MacDonald, L. Pfeiffer, and K. West, Surface science **263**, 446 (1992).
 - [15] T. Gramila, J. Eisenstein, A. MacDonald, L. Pfeiffer, and K. West, Physica B: Condensed Matter **197**, 442 (1994).
 - [16] P. Solomon and B. Laikhtman, Superlattices and Microstructures **10**, 89 (1991).
 - [17] J. Eisenstein, Superlattices and microstructures **12**, 107 (1992).
 - [18] J. Li, T. Taniguchi, K. Watanabe, J. Hone, A. Levchenko, and C. Dean, Physical review letters **117**, 046802 (2016).

- [19] K. Lee, J. Xue, D. C. Dillen, K. Watanabe, T. Taniguchi, and E. Tutuc, Physical review letters **117**, 046803 (2016).
- [20] P. Debray, V. Zverev, O. Raichev, R. Klesse, P. Vasilopoulos, and R. Newrock, Journal of Physics: Condensed Matter **13**, 3389 (2001).
- [21] M. Yamamoto, M. Stopa, Y. Tokura, Y. Hirayama, and S. Tarucha, Science **313**, 204 (2006).
- [22] D. Laroche, G. Gervais, M. Lilly, and J. Reno, Science **343**, 631 (2014).
- [23] Y. Tang, A. Tylan-Tyler, H. Lee, J.-W. Lee, M. Tomczyk, M. Huang, C.-B. Eom, P. Irvin, and J. Levy, Advanced Materials Interfaces , 1900301 (2019).
- [24] A. Keller, J.-S. Lim, D. Sánchez, R. López, S. Amasha, J. Katine, H. Shtrikman, and D. Goldhaber-Gordon, Physical review letters **117**, 066602 (2016).
- [25] N. Giordano and J. Monnier, Physical Review B **50**, 9363 (1994).
- [26] X. Huang, G. Bazàn, and G. H. Bernstein, Physical review letters **74**, 4051 (1995).
- [27] E. Shimshoni, Physical Review B **51**, 9415 (1995).
- [28] A. Kamenev and Y. Oreg, Physical Review B **52**, 7516 (1995).
- [29] J.-M. Duan and S. Yip, Physical review letters **70**, 3647 (1993).
- [30] A. Levchenko and A. Kamenev, Physical review letters **101**, 216806 (2008).
- [31] B. Narozhny and I. Aleiner, Physical review letters **84**, 5383 (2000).
- [32] C. Cen, S. Thiel, G. Hammerl, C. Schneider, K. Andersen, C. Hellberg, J. Mannhart, and J. Levy, Nature materials **7**, 298 (2008).
- [33] K. A. Brown, S. He, D. J. Eichelsdoerfer, M. Huang, I. Levy, H. Lee, S. Ryu, P. Irvin, J. Mendez-Arroyo, C.-B. Eom, M. C. A., and L. Jeremy, Nature communications **7**, 10681 (2016).
- [34] M. Tinkham, J. Free, C. Lau, and N. Markovic, Physical Review B **68**, 134515 (2003).
- [35] O. Raichev and P. Vasilopoulos, Physical Review B **61**, 7511 (2000).
- [36] N. Reyren, S. Thiel, A. Caviglia, L. F. Kourkoutis, G. Hammerl, C. Richter, C. Schneider, T. Kopp, A.-S. Rüetschi, D. Jaccard, M. Gabay, D. A. Muller, J.-M. Triscone, and J. Mannhart, Science **317**, 1196 (2007).
- [37] A. Nethwewala, H. Lee, M. Briggeman, Y. Tang, J. Li, J. Lee, C.-B. Eom, P. R. Irvin, and J. Levy, Nanoscale Horizons **4**, 1194 (2019).

Supplemental Material

In the supplement materials, Fig. S1 shows the typical two-terminal ($R_{2T,2}$) and four-terminal resistance (R_{22}) from a nanowire. The superconducting-normal transition at small bias showing up in both two-terminal and four-terminal resistance comes from the nanowire. The extra superconducting-normal transitions at larger biases in $R_{2T,2}$ come from wires connecting the nanowire and the electrode.

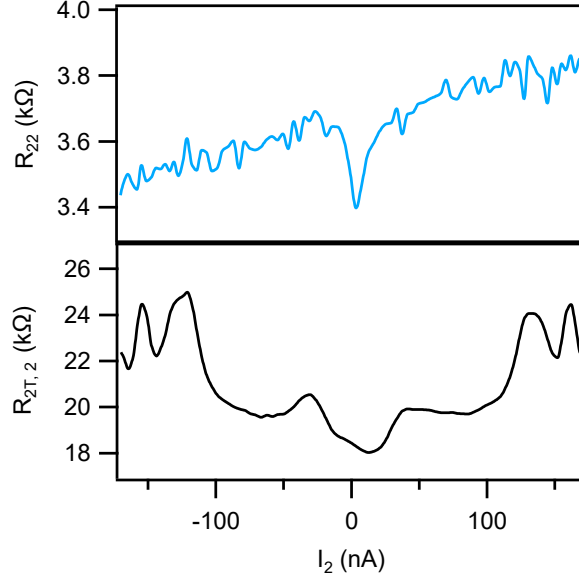


FIG. S1. Typical two-terminal resistance and four-terminal resistance from a nanowire. Top panel: Four-terminal resistance R_{22} and superconducting-normal transition from the nanowire only shows up at small bias from ± 20 nA. Bottom panel: Two-terminal resistance $R_{2T,2}$. Besides the superconducting-normal transition at small bias extra superconducting-normal transitions show up at larger bias ± 110 nA and ± 150 nA. Superconducting-normal transitions at larger bias come from wires connecting the nanowire and electrodes.